Available online at www.sciencedirect.com
ScienceDirect
Signal Processing 88 (2008) 1–18
SIGNAL PROCESSING
www.elsevier.com/locate/sigpro

Improved Wigner–Ville distribution performance based on DCT/DFT harmonic wavelet transform and modified magnitude group delay

S.V. Narasimhan[a,*], A.R. Haripriya[b], B.K. Shreyamsha Kumar[b]

[a]*Digital Signal Processing Systems Group, Aerospace Electronics and Systems Division, National Aerospace Laboratories, Bangalore 560017, India*
[b]*Department of ECE, National Institute of Technology Karnataka (NITK), Surathkal 575025, India*

Received 21 July 2006; received in revised form 22 June 2007; accepted 28 June 2007
Available online 10 July 2007

Abstract

A new Wigner–Ville distribution (WVD) estimation is proposed. This improved and efficient WVD is based on signal decomposition (SD) by DCT or DFT harmonic wavelet transform (DCTHWT or DFTHWT) and the modified magnitude group delay (MMGD). The MMGD processing can be either in fullband or subband. The SD by DCTHWT provides better quality low leakage decimated subband components. The concatenation of WVDs of the subbands results in an overall WVD, significantly free from crossterms and Gibbs ripple. As no smoothing window is used for the instantaneous autocorrelation (IACR), MMGD removes or reduces the Gibbs ripple preserving the frequency resolution achieved by the DCT/DFT HWT. The SD by DCTHWT compared to that of DFTHWT, has improved frequency resolution and detectability. These are due to the symmetrical data extension and the consequential low leakage (bias and variance). As the zeros due to the associated white noise are removed by the MMGD effectively in subband domain than in fullband, the proposed WVD based on subband has a better noise immunity. Compared to fullband WVD, the subband WVD is computationally efficient and achieves a significantly better: frequency resolution, detectability of low-level signal in the presence of high-level one and variance. The SD-based methods, however cannot bring out the frequency transition path from band to band clearly, as there will be gap in the contour plot at the transition. For the proposed methods, the heart rate variability (HRV) real data is also considered as an example.
© 2007 Elsevier B.V. All rights reserved.

Keywords: Wigner–Ville distribution; DFT harmonic wavelet transform; DCT harmonic wavelet transform; Signal decomposition; Modified magnitude group delay function; Fullband and subband processing; Heart rate variability (HRV) data

1. Introduction

The Wigner–Ville distribution (WVD) is used for the analysis of nonstationary signals. In practice, the pseudo-WVD (PWVD), the Fourier transform of the instantaneous autocorrelation (IACR) computed only for a finite number of lags, is used. In the PWVD, to overcome the IACR truncation effect

*Corresponding author. Tel.: +91 080 25086521; fax: +91 080 25268546.
E-mail address: narasim@css.cmmacs.ernet.in (S.V. Narasimhan).

0165-1684/$ - see front matter © 2007 Elsevier B.V. All rights reserved.
doi:10.1016/j.sigpro.2007.06.013

(Gibbs ripple), a smoothing *window function* is used. For a given lag length, the windowing *deteriorates the frequency resolution*. For a multicomponent signal, the WVD being quadratic in nature introduces undesired crossterms. The crossterms can be reduced by time smoothing *but only at the cost of time resolution.* To suppress crossterm effectively, to improve the frequency resolution and to maintain the desired time–frequency representation (TFR) properties, many distributions are proposed with varying degree of success. The prominent are: the Choi–William's, Cone–Kernel and reduced interference Kernel [1].

Recently, a WVD based on signal decomposition (SD) and modified magnitude group delay—MMGD (FBWVD), has been proposed [3]. The SD is realized by a perfect reconstruction filter bank (PRFB). The Gibbs ripple due to IACR truncation, manifests as zeros close to the unit circle. The MMGD removes these zeros without applying any smoothing window function [4]. The removal of zeros doest not disturb the signal pole locations and hence preserves the frequency resolution of a rectangular window.

The PRFB reduces the crossterms effect for a multicomponent signal, as the overall IACR is achieved by the summation of their individual IACRs computed separately [2]. However the SD by PRFB and computation of the individual IACRs at *the original sampling rate*, *are computationally intensive*. The decimation for the IACR, may appear to reduce computations. This is not so as WVD requires both decimation and interpolation operations, which by themselves are computationally intensive.

The DFT harmonic wavelet transform (DFTHWT) [5] can decompose and reconstruct the signal, without *directly* performing the decimation and interpolation operations. In DFTHWT, these operations are built in. As the decimated components are readily available in the frequency domain, certain type of processing, like group delay is directly applicable. This makes the overall algorithm simple and computationally efficient [9].

The DFTHWT is good as long as no processing of the components is involved prior to inverse transformation. It may also be tolerable for a signal with well-separated frequency components of high magnitude. To get improved WVD, after SD, it is required to process individual subband components differently. In such a case, decomposing the signal based on DFTHWT and processing the resulting subbands may not be very effective. This is because the signal energy from one component to another has *already leaked* during the FT computation.

As the DCT extends the signal symmetrically, it results in a significant reduction in abruptness of truncation and hence the leakage effect. This is due to smooth transition from one period to another (built-in periodicity) in DCT. It appears as if there is *no windowing and no side lobes to enhance the Gibbs and leakage effects* [10a]. It also improves the detection ability of a smaller magnitude component in the presence of a larger one. These facts motivated the authors to extend the desirable spectral properties of the DCT [10b] to harmonic wavelet transform (HWT) by grouping the DCT coefficients [11], instead of DFT coefficients.

This paper proposes a new efficient approach to improve the performance of WVD. This is based on the SD by DCT/DFTHWT and MMGD function. The SD by DCT/DFT HWT and the MMGD remove/reduce the existence of the crossterms and the Gibbs ripple due to truncation of the IACR, respectively. The application of MMGD to subband components improves both the frequency resolution and noise immunity compared to those of fullband. The SD by DCTHWT is advantageous over that by PRFB and DFTHWT as it results in reduction in computations, improved frequency resolution and signal detection ability.

2. Wigner–Ville distribution [1]

The WVD of an analytic signal $x(t)$is given by

$$W_x(t,\omega)=\int_{-\infty}^{\infty} r(t,\tau)\,\mathrm{e}^{-\mathrm{j}\omega\,\tau}\,\mathrm{d}\tau, \tag{1}$$

where $r(t,\ \tau)=x(t+\tau/2)\ \ x^*(t-\tau/2)$ is called the IACR function/Wigner kernel. From the computational point of view, the IACR can be considered only for a finite number of lags. This implies application of an inevitable rectangular window, which results in the Gibbs ripple effect. A smoothing window is applied to the IACR to reduce the Gibbs ripple and the resulting WVD is known as Pseudo-Wigner–Ville distribution (PWVD), given by

$$\mathrm{PW}_x(t,\omega)=\int_{-\infty}^{\infty} x(t+\tau/2)x^*(t-\tau/2)h^2(\tau/2)\,\mathrm{e}^{-\mathrm{j}\omega\tau}\,\mathrm{d}\tau. \tag{2}$$

The window function $h^2(\tau/2)$ reduces the Gibbs ripple. But it results in a reduction in frequency

resolution as it *eats away* the correlation function at higher lags.

The WVD introduces crossterms for multicomponent signals and this is due to the quadratic nature of WVD [1]. The crossterm has a large magnitude. Further, there will be a crossterm with every pair of components of the signal. Hence the interpretation of WVD becomes difficult. Since the crossterm oscillates in time, smoothing the WVD in time attenuates the crossterm and enables meaningful interpretation of the TFR. *But this crossterm reduction is only at the expense of time resolution.* The smoothing in time for crossterms and in frequency for the lag window can be considered as a two-dimensional (2D) convolution of the WVD with a smoothing kernel [1]. The kernel determines the properties of the distribution. The use of different smoothing kernels results in a class of distribution, called the *Cohen's class*. But the WVD obtained by using common smoothing kernel (other than rectangular) do not satisfy some of the TFR properties [1].

3. Harmonic wavelet transform [5]

The wavelet transform (WT) of a signal is generally realized in time domain by a two-channel PRFB using a dyadic structure. Newland introduced the HWT [5] and this enables the wavelet/wave packet implementation in the frequency domain. For a wavelet function $w(t)$, the WT coefficient $a(t)$ of a signal $x(t)$ is

$$a(t) = \int_{-\infty}^{\infty} x(\tau) w(t+\tau)\,\mathrm{d}\tau. \tag{3}$$

In terms of Fourier transform,

$$A(\omega) = X(\omega)\, W^*(\omega)$$

$$a(t) = F^{-1}[X(\omega) W^*(\omega)]. \tag{4}$$

That is, the WT coefficients can be computed using FFT algorithm by Eq. (4) using $X(\omega)$ with $W(\omega)$ for different wavelet functions. Specifically for the HWT of Newland [5], $W(\omega)$ is very simple and it is zero except over a finite band $[\pi/p, \pi/q]$, where p, q can be real numbers, not necessarily integers.

The multiplication of $X(\omega)$ by $W^*(\omega)$ while using the discrete Fourier transform (DFT), is equivalent to *grouping of the DFT coefficients* of a signal in a dyadic fashion. The inverse DFT of each group yields harmonic wavelet transform coefficients (HWC) [5]. The inverse HWT can be achieved by deriving the complete DFT by proper concatenation of the DFT coefficient groups obeying the possible DFT conjugate symmetry and taking its inverse DFT. For HWT, the above choice of $W(\omega)$ though compact in the frequency domain, is of infinite duration in time domain. This can be overcome by using a proper smoothing weighing function for the grouped DFT coefficient sequence.

3.1. DCT harmonic wavelet transform (DCTHWT) [11]

The harmonic wavelet transform based on DFT (DFTHWT) as already explained has the features of simplicity with its built-in decimation and interpolation operations. The very purpose of orthogonal WT is to decompose the signal into *orthogonal components*, which are independent so that their further processing will not affect one another. However, this is not so with *the DFTHWT, as the Fourier coefficients, which are already affected by leakage, are grouped.* The processing on any band will affect the neighboring bands indirectly as the leaked energy also gets processed.

Therefore to utilize the features of the harmonic wavelet transform, *it is necessary to reduce the leakage effects and in this direction, use of DCT instead of DFT is an important step*. This is because the DCT *extends the data symmetrically*. Here there is a smooth transition from one DCT period to the other and *the discontinuity, which is the root cause for leakage, is significantly removed*. Compared to the DFT, the DCT has a better frequency resolution due to data extension and this enables DCT to resolve the closely spaced spectral components.

The DCT of a N point signal $x(n)$, $n = 0, 1, 2, \ldots(N-1)$; is defined as the DFT of a $2N$ point symmetrically extended signal $y(n)$

$$y(n) = \begin{cases} x(n), & 0 \leqslant n \leqslant N-1, \\ x(2N-1-n), & N \leqslant n \leqslant 2N-1, \end{cases} \tag{5}$$

where $y(n)$ is even symmetric with respect to the point $[N-(1/2)]$. This leads to DCT and is given by

$$C_x(k) = \begin{cases} \sum_{n=0}^{N-1} 2x(n)\cos\frac{\pi k(2n+1)}{2N}, & 0 \leqslant k \leqslant N-1, \\ -C_x(2N-k), & N \leqslant k \leqslant 2N-1. \end{cases} \tag{6}$$

Here, the DCT has been derived from the DFT.

With the DFTHWT, in getting the decimated subband component signal and in signal reconstruction, the conjugate symmetry of the DFT has to be accounted. The component signals can also be complex. But with the DCTHWT as the coefficients are real and the symmetry is built-in, no conjugation symmetry operation is required. Thus the DCTHWT is simpler and provides better performance.

4. MMGD for complex signals [6,7]

If $x(n)$ is a minimum phase complex signal with $X(\omega)$ as its Fourier transform,

$$\ln|X(\omega)| = \sum_{n=0}^{\infty}[c_R(n)\cos\omega n + c_I(n)\sin\omega n], \tag{7}$$

$$\theta(\omega) = \sum_{n=0}^{\infty}[-c_R(n)\sin\omega n + c_I(n)\cos\omega n]. \tag{8}$$

The group delay $\tau(\omega)$, the negative derivative of phase $\theta(\omega)$, is given by

$$\begin{aligned}\tau(\omega) &= -\frac{\partial}{\partial\omega}[\theta(\omega)] \\ &= \sum_{n=0}^{\infty}[nc_R(n)\cos\omega n + nc_I(n)\sin\omega n].\end{aligned} \tag{9}$$

If $nc(n)$ conjugate symmetric [6],

$$\tau(\omega) = \mathrm{FT}[nc(n)]. \tag{10}$$

Here, $\theta(\omega)$ is the unwrapped phase and $c(n)$ ($c(n) = c_R(n) + jc_I(n)$) are cepstral coefficients. The cepstral coefficients $c_R(n)$ and $c_I(n)$are derived from magnitude information (Eq. (7)). $\tau(\omega)$ is obtained using these coefficients and hence is called magnitude group delay (MGD).

The ripple/variance in a spectrum can be due to (1) signal truncation effect, (2) associated white noise, (3) the input white noise that drives a system in generating the signal and (4) any of the possible combinations. These introduce zeros close to the unit circle. Application of a smoothing window to the signal, results in pulling the signal poles and zeros towards the origin in addition to the zeros near the unit circle. Hence the reduction in variance due to signal windowing is only at the cost of frequency resolution. The MGD modification given in [3,4] only removes the zeros close to the unit circle without disturbing the signal or system poles. Hence the use of modified MGD enables variance reduction preserving the frequency resolution of the rectangular window.

For a complex signal $x(n)$, if $X(\omega) = N(\omega)/D(\omega)$, then $D(\omega)$ corresponds to the signal peaks and $N(\omega)$ mainly contributes to the ripples/variance [4,7]. Hence the ripple/variance of $X(\omega)$ can be removed by dividing it by $N(\omega)$. However, this may result in singularity problems. In the group delay domain, the same operation can be realized by multiplication avoiding any singularity. The MGD of $X(\omega)$, $\tau(\omega)$ is

$$\tau(\omega) = \tau_N(\omega) - \tau_D(\omega), \tag{11}$$

where $\tau_N(\omega)$ and $\tau_D(\omega)$ are the MGDs corresponding to $N(\omega)$ and $D(\omega)$, respectively. The group delay of signal $v(n)$ is given by

$$\tau_v(\omega) = \frac{V_R(\omega)Y_R(\omega) + V_I(\omega)Y_I(\omega)}{|V(\omega)|^2},$$

where $y(n) = nv(n)$, $V(\omega) = \mathrm{FT}[v(n)]$, $Y(\omega) = \mathrm{FT}[y(n)]$. Further $V_R(\omega)$, $Y_R(\omega)$ are the real and $V_I(\omega)$, $Y_I(\omega)$ are the imaginary parts of $V(\omega)$ and $Y(\omega)$, respectively. Representing the numerator by $K(\omega)$,

$$\tau_v(\omega) = \frac{K(\omega)}{|V(\omega)|^2}.$$

With this representation, Eq. (11) can be written as

$$\tau(\omega) = \frac{K_N(\omega)}{|N(\omega)|^2} - \frac{K_D(\omega)}{|D(\omega)|^2}. \tag{12}$$

For the simplicity of explanation, $K_N(\omega)$ and $K_D(\omega)$ can be considered as constants [4]. For zeros close to the unit circle, $|N(\omega)|^2$ will be very small and for signal poles which are relatively far from unit circle, $|D(\omega)|^2$ is large. Hence in Eq. (12) for $\tau(\omega)$, the contribution is mainly from the first term and this masks the signal peaks which are due to second term. This masking effect of these zeros can be reduced by multiplying $\tau(\omega)$ by $|N(\omega)|^2$. Hence, the modified MGD (MMGD) $\tau_{mo}(\omega)$, is

$$\tau_{mo}(\omega) = K_N - \frac{K_D}{|D(\omega)|^2}|N(\omega)|^2. \tag{13}$$

The estimate of $|N(\omega)|^2$, $|\hat{N}(\omega)|^2$ is given by [4],

$$|\hat{N}(\omega)|^2 = \frac{|X(\omega)|^2}{|\bar{X}(\omega)|^2}, \tag{14}$$

where $|\bar{X}(\omega)|^2$ is the smoothed power spectrum of the signal obtained by the truncated cepstral coefficient sequence of $x(n)$.

5. Improved WVD based on SD by DFT/DCTHWT and MMGD processing in fullband/subband

In the proposed method, the multicomponent signal is decomposed into its components by DCT/DFT HWT and their WVDs are computed. The Gibbs ripple in each WVD slice is removed/reduced by applying the MMGD. The MMGD can be applied for the fullband WVD [8] or to the WVD of the subband decimated signals and the processed subband WVDs are concatenated to get the fullband WVD. The subband MMGD processing has an improved performance over that of the fullband.

5.1. SD by DCT/DFT HWT

To avoid the occurrence of crossterms due to the quadratic nature of the WVD, a multicomponent signal is decomposed into its components by DCTHWT where the DCT coefficients are grouped uniformly. The analytic signals of the IDCT of these groups are considered to get the desired WVD.

The SD using DCTHWT for a signal $\{x(n)\} = \{x(0),\ x(1),\ \ldots,\ x(7)\}$ is illustrated. Let $\{X(0),\ X(1),\ \ldots,\ X(7)\}$ be the DCT coefficients of the signal considered. The array $\{X(0),\ X(1),\ \ldots,\ X(7)\}$ is split into two uniform bands,

$$[X_1] = [X(0),\ X(1),\ X(2),\ X(3)]$$

and

$$[X_2] = [X(4),\ X(5),\ X(6),\ X(7)].$$

The inverse DCT of these bands result in

$$\{x_1(n)\} = \{x_1(0),\ x_1(1),\ x_1(2),\ x_1(3)\}$$

and

$$\{x_2(n)\} = \{x_2(4),\ x_2(5),\ x_2(6),\ x_2(7)\}$$

and these give respective DCTHWT coefficients which are already decimated because of built-in decimation of the harmonic wavelet transform. However as the WVD is computed at the original signal sample instants, *it is necessary to preserve the original sampling time instants, for these components derived from* DCTHWT. This is realized by zero padding to DCT coefficients sequence of each band. In this case, zeros are added to double their lengths. The new DCT bands are

$$[X_{\mathrm{d}1}] = [X(0),\ X(1),\ X(2),\ X(3),\ 0,\ 0,\ 0,\ 0]$$

and

$$[X_{\mathrm{d}2}] = [X(4),\ X(5),\ X(6),\ X(7),\ 0,\ 0,\ 0,\ 0].$$

The inverse DCT of these bands are

$$\{x_{d1}(n)\} = \{x_{d1}(0),\ x_{d1}(1),\ x_{d1}(2)\ldots x_{d1}(7)\}$$

and

$$\{x_{d2}(n)\} = \{x_{d2}(0),\ x_{d2}(1),\ x_{d2}(2)\ldots x_{d2}(7)\}.$$

These give respective DCTHWT coefficients at the *original signal sampling rate*. The reconstruction from DCTHWT coefficients is just the reverse process of the decomposition and is obtained by taking the DCT of $\{x_{d1}\}$ and $\{x_{\mathrm{d}2}\}$ to get $[X_{d1}]$ and $[X_{d2}]$, respectively.

$$[X_{d1}] = \{X(0),\ X(1),\ X(2),\ X(3)\}$$

and

$$[X_{d2}] = \{X(4),\ X(5),\ X(6),\ X(7)\}.$$

The concatenation of $[X_{d1}]$ and $[X_{d2}]$ at their respective positions is, $[X_{d1},\ X_{d2}]$. That is, $[X_{d1},\ X_{d2}] = [X(0),\ X(1),\ X(2),\ X(3),\ X(4),\ X(5),\ X(6),\ X(7)]$ gives the fullband DCT, $[X]$ and its inverse DCT gives the original signal. As DCT is real there is no need to do the conjugate operation in placing the coefficients symmetrically. (In DCT-II algorithms used in practice, the symmetrical placement is not needed and the inverse DCT-II gives the one sided signal.)

To get component WVDs, the IACR of the analytic signal for each group $\{x_{d1}(n)\}$ and $\{x_{d2}(n)\}$ is considered.

For a SD of M components, *the IACR is computed at every input signal instant but at decimated lags. That is, the lags are once in every* Mth (*in this example* $M = 2$) *data sample so that the effective lag length is decimated by a factor* M *and this reduces the computational complexity*. For the ith component the IACR is given by

$$r_i(n,k) = x_i(n+Mk)x_i^*(n-Mk), \quad k = 1,2,3,\ldots K.$$

Here, K is the maximum lag value and M is the number of bands, considered.

The individual WVDs for the decomposed components are obtained by taking the FT of their IACR. By plugging back these individual component WVDs in their corresponding position, the complete WVD of the original signal is derived (Fig. 1, for $N = 8$). The use of analytic signal for the WVD requires the processing of complex signals.

The SD by DFTHWT is similar to that of DCTHWT and here the DFT coefficients are grouped obeying the DFT symmetry (as for as possible since at some stages of decomposition, the

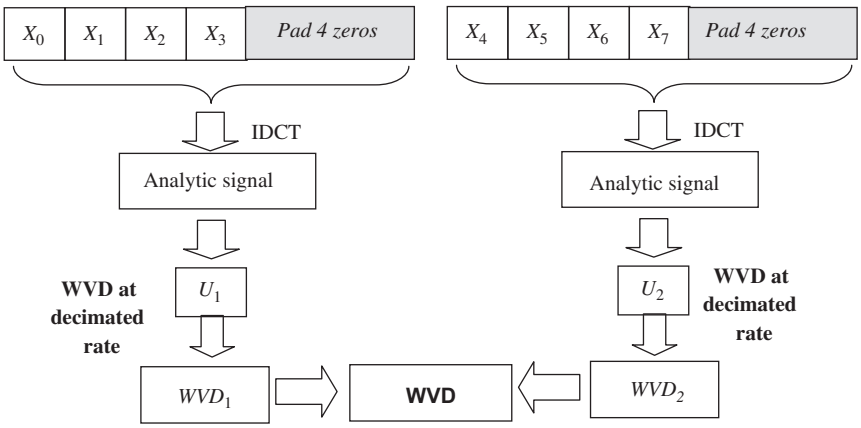

Fig. 1. Computation of WVD by DCTHWT.

symmetry about a real coefficient like in normal DFT may not be possible).

5.2. Improved WVD based on SD by DCT/DFT by MMGD processing in fullband (IFCTWVD/IFFTWVD) and subband (ISCTWVD/ISFTWVD)

For a given lag length, as the lag windowing eats away the correlation function at higher lags, it reduces the frequency resolution of the PWVD. For the WVD, the input is an analytic signal and this is complex. Therefore the MMGD for complex signals (reviewed in Section 4) is used for the Gibbs ripple reduction preserving its original frequency resolution. In WVD, as only the ripple on the floor is to be removed, the modified group delay is given by [3]

$$\tau_{m\Delta}(\omega) = \tau_m(\omega)\left|\Delta(\omega)\right|^2, \tag{15}$$

where $\Delta(\omega)$ represents the fluctuating part of $X(\omega)$ and this is given by

$$\hat{N}(\omega) = \frac{X(\omega)}{\bar{X}(\omega)} = \left[1 + \frac{\Delta(\omega)}{\bar{X}(\omega}\right]. \tag{16}$$

To apply the MMGD for the present TFR, the starting point is the fullband WVD slice obtained after SD. From the positivity ensured WVD [3], the equivalent magnitude spectrum computed is used to derive the MGD $\tau_m(\omega)$ [6]. The positivity ensured WVD slice is realized by multiplying its IACR at zeroth lag value by a factor much greater than unity. This results in raising the floor level of the WVD. The improved fullband WVD slice is obtained from $\tau_{m\Delta}(\omega)$ (using Eqs. (13) and (10)). This will be not only free from the ripple effect but also has better frequency resolution.

This procedure for a single WVD slice has to be repeated for every WVD slice to get the complete WVD (IFCTWVD/IFFTWVD), which is free from both crossterm and ripple and better frequency resolution. As the MMGD also removes the zeros due to the associated white noise, the WVD indirectly achieves better noise immunity.

For applying MMGD in subbands (ISCTWVD/ISFTWVD), for a particular subband, the IACR function is computed at each time instant. Further, from the positivity ensured WVD, the MMGD $\tau_{m\Delta}(\omega)$ and hence the improved component WVD are computed. The complete WVD slice is obtained by concatenating the component WVDs at their respective positions. To get the complete WVD, this procedure is repeated for every time instant. In general, any processing in subbands is more effective as frequency resolution and signal to noise ratio are improved by a factor corresponding to the decimation. This is due to spectral expansion and or spectral peaks separation into different subbands (that reduces mutual effect of spectral peaks on one another). The MMGD processing is not an exception to this. Therefore the MMGD provides a better performance in subbands than in fullband making the ISCTWVD/ISFTWVD to have an edge over IFCTWVD/IFFTWVD.

The SD will remove/reduce the crossterms of the WVD without time smoothing and preserves the time resolution. The MGD processing of the fullband WVD removes/reduces the Gibbs ripple preserving the frequency resolution of the rectangular window. The MGD processing of the individual subband WVD provides better frequency resolution, improvement in signal to noise ratio resulting in a better detectability of a weak signal in

the presence of strong one. Unlike the methods which do not use the SD to remove crossterms, *the WVD methods based on SD cannot bring out properly the signal frequency transition path from one band to another*. But the methods not based on SD, suffer from limitations like time resolution due to time smoothing and trade off between crossterms suppression and frequency resolution as in Choi–Williams distribution [1]. In the proposed methods, the IACR of the component signals are computed *only for a limited number of lags* and the values for higher lags are treated as zero. The FT of such an approximate IACR cannot reproduce the original spectrum. The autocorrelation coefficients are the Fourier coefficients of the spectral pattern and the removal higher order coefficients, result in a smoothed boundary rather than a sharp one. Hence the spectral values fall off as the band transition is reached. This aspect of the SD-based WVD methods was not known earlier when they were reported [2,3,8]. Hence the desirable features of the SD-based WVD can be fully utilized in cases where there is no desired information across band transitions.

5.2.1. Algorithm

Step 1: Obtain the component signals and compute the IACR for each component as explained in Section 5.1.

For IFCTWVD/IFFTWVD

Step 2: Compute FT of each IACR component to get the component WVD slice and concatenate to get the full WVD slice.

Step 3: To get positivity ensured WVD: take the inverse FT of the full WVD slice and this gives the complete IACR for that instant and raise the floor level of the WVD by multiplying the IACR zeroth lag value by a factor much greater than unity (say 5000).

Step 4: Compute the MMGD for this IACR and get the *IFCTWVD/IFFTWVD* slice.

For ISCTWVD/ISFTWVD

Step 2: To get positivity ensured component WVD, raise the floor level of each component WVD by multiplying their respective IACR zeroth lag value by a factor much greater than unity (say 5000).

Step 3: Compute the MMGD for each component IACR and get the modified component WVD slice.

Step 4: Concatenate the component WVDs to get complete WVD slice.

Step 5: To get the complete WVD for fullband or subband, repeat the respective above steps—2 to 4, for all the sample time instants.

5.3. Computational complexity

The computational complexity (Table 1) is considered in three stages of the WVD. Here M is number of subbands, nf is filter length and dp is the signal length.

(i) The SD using PRFB or DFTHWT or DCTHWT in terms of multiplication and additions: FBWVD requires the M convolutions to compute filter bank outputs. The computational complexity of a convolution is more compared to FFT and DCT. As the number of subbands increases, the FBWVD

Table 1
Computational complexity by different methods

Method	For SD No. of multiplications, no. additions	For IACR No. of multiplications	No. of FFTs (IACR to WVD slice)
WVD	–	$dp*(2L+1)$: 8448	dp
FBWVD	$[nf*dp]*M$: 65,536	$dp*M*(2L+1)$: 16,896	dp
(without MMGD)	$[nf*dp-(nf+dp-1)]*M$: 64,770		
IFTWVD	$\left[2*dp*\log_2(dp)\right]*(M+1)$: 12,288	$dp*M*(2L/M+1)$: 8704	dp
(without MMGD)	$\left[2*dp*\log_2(dp)\right]*(M+1)$: 12,288		
ICTWVD	$\left[\left[dp*\log_2(dp)\right]-\frac{3*dp}{2}+4\right]*2*(M+1)$: 3336	$dp*M*(2L/M+1)$: 8704	dp
(without MMGD)	$\left[\left[3*dp*\left(\log_2(dp)-1\right)/2\right]+2\right]*2*(M+1)$: 16,140		

For the parameter values are $dp=256$, $N=128$, $M=2$, $L=16$, $nf=128$.

Table 2
Reduction (%) in computations with respect to PRFB

Operations	SD by DFTHWT and IACR together (%)	SD by DCTHWT and IACR together (%)
For multiplications	74.5	85.4
For additions	81	69.5

requires more number of computations compared to IFTWVD and ICTWVD. Between IFTWVD and ICTWVD, the latter requires less number of computations as it involves only real operations. In ICTWVD, sparse factors algorithm has been considered in arriving the DCT computational complexity of SD [12].

(ii) IACR computation in terms of multiplication: As IACR is computed at a decimated rate for improved fullband WVD (IFWVD) and improved subband WVD (ISWVD), it requires less computations than that by FBWVD.

(iii) Number of FFTs required to compute the complete WVD: The FBWVD, IFWVD and ISWVD require *dp FFTs* to get *dp* WVD slices from the IACR function.

As seen from Table 1, for the proposed method, the SD by DCTHWT has 72.8% reduction in computations in terms of multiplications and it requires 30% more additions, compared to that by DFTHWT (for the parameters in Table 1).

Table 2 indicates the percentage of computation reduction in terms of multiplications and additions compared to PRFB. For using MMGD, the IFWVD TFR slice requires 8 FFTs. However, for the ISWVD TFR slice requires equivalent 6 FFTs. On the whole, the ISWVD is computationally very efficient.

6. Simulation results

The performance of the proposed IWVD algorithms is illustrated for crossing chirp and sinusoidal chirp signals. In these examples, the parameters used are: number of lags = 33, data points = 256, DFT length = 128. To ensure positivity of the PSD, the IACR at the zeroth lag is increased by a factor of 5000. For the estimation of $|\Delta(\omega)|^2$ the number of cepstral coefficients used, for crossing chirp signal are: 4 for fullband MMGD processing and 3 for subband MMGD processing and for sinusoidal chirp signal are: 4 for fullband MMGD processing and 2 for subband MMGD processing.

For a crossing chirp signal $\cos[2(566-0.6n)nT_s+\cos[2(76\pi+0.6n)nT_s]$, the IWVD is free from Gibbs ripple and crossterms. The IWVD is free from Gibbs ripple but preserves the frequency resolution of the rectangular window. Specifically the proposed ISCTWVD has a better frequency resolution than those of other algorithms, due to SD by DCTHWT and MMGD processing in subbands (Fig. 2). For the fullband processing, contour plots show discontinuity. This is due to the variations in the magnitude of the envelope of the TFR. But for the proposed subband processing methods, the envelope magnitude level is maintained resulting in a continuous contour plots (Fig. 2). For ISCTWVD only, the spectral peaks decay sharply. This results in a wider flat region, which is not so with other methods (specifically ISFTWVD). This indicates that its frequency resolution is better.

For the crossing chirp signal in the presence of white noise (SNR = 6 dB), the ridge type of effect is observed in all cases, but it is reduced in case of ISCTWVD (Fig. 3). For ISCTWVD (Fig. 3), in the region between the crossing chirps (along the frequency axis), the floor is clean, the contour is narrower and continuous; compared to the other methods. This indicates the superior performance of DCT and subband processing even in presence of noise.

In this example, the SD by splitting signal frequency band into two bands at a frequency where the two chirps cross each other, removes the crossterm. But along each chirp in the neighborhood of band splitting, the spectral magnitude of the chirp is reduced (as explained in Section 5.2). In view of this, there is a discontinuity along each chirp in the contour plot. Specifically for the inner most contour (which corresponds to the highest magnitude), this discontinuity is very explicit indicating that there is a significant reduction in spectral magnitude due to SD.

For 2 nonstationary sinusoidal chirp signals $\sin[2\pi\{94+0.64\sin(n/16)\}nT_s]$ and $\sin[2\pi\{160+1.08\sin(n/17)\}nT_s]$, the IWVD obtained by different algorithms are shown in Fig. 4. It is evident that resolvability of 2 peaks (sharpness of the peaks) is better for subband processing than for fullband processing. Also from contour plots, it can be observed that there is better continuity in case of subband than that in fullband. In the case of DCT-based SD, flat region between 2 peaks is more

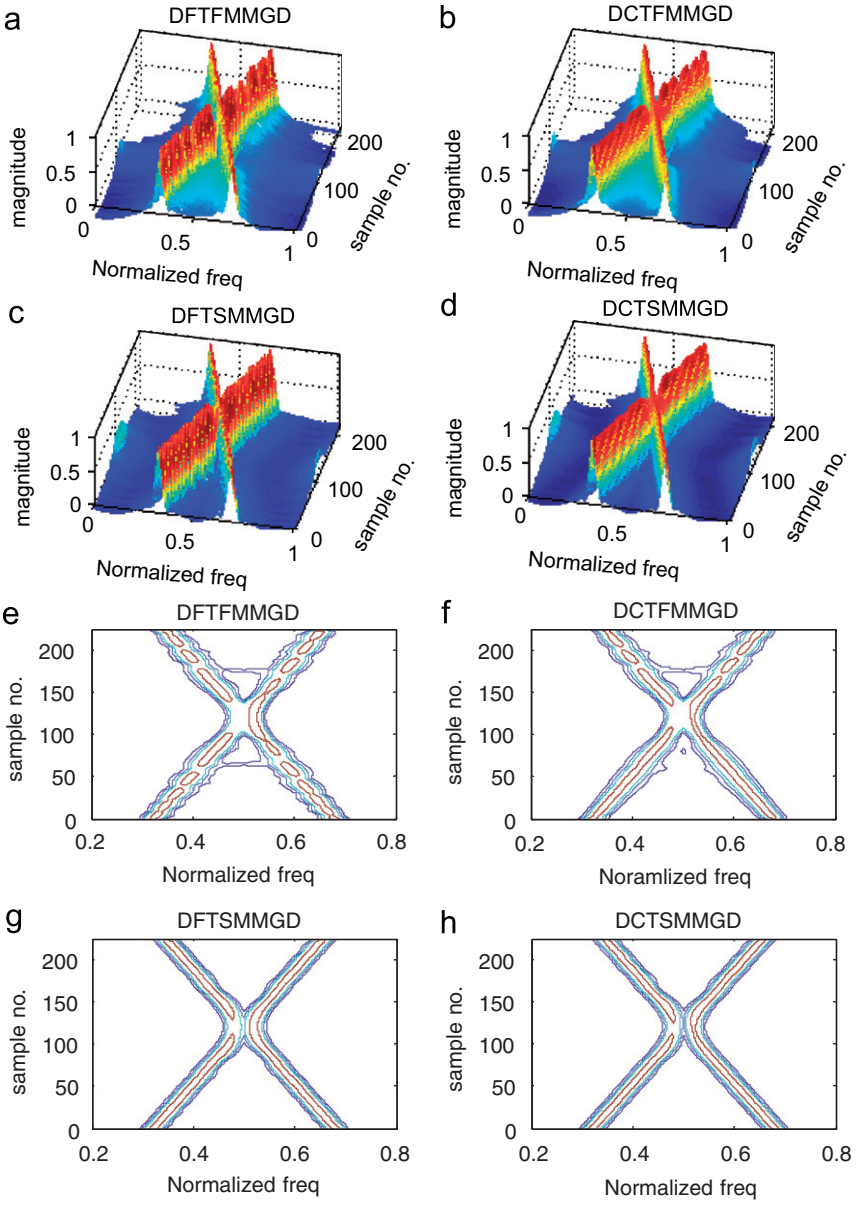

Fig. 2. TFR of a crossing chirp signal by (a) IFFTWVD, (b) IFCTWVD, (c) ISFTWVD, (d) ISCTWVD, and (e)–(h) contours of plots (a)–(d).

compared to that of DFT-based SD indicating its better frequency resolution.

For the nonstationary sinusoidal chirp signals in presence of white noise (SNR = 16 dB), the IWVD obtained by different algorithms are shown in Fig. 5. From this it is clear that even with noise, the resolvability of 2 peaks is better in case subband processing than in fullband processing. In this noisy case for the DCT-based SD, the flat region in between 2 peaks is more than in case of DFT-based SD.

To evaluate the performance of the different methods considered, average sum sample variance (ASSV) is used as the performance index and is given by

$$\mathrm{ASSV} = \frac{1}{(M^{*}N)} \sum_{i=1}^{M} \sum_{j=1}^{N} \mathrm{TFR}_{\mathrm{var}}(i,j),$$

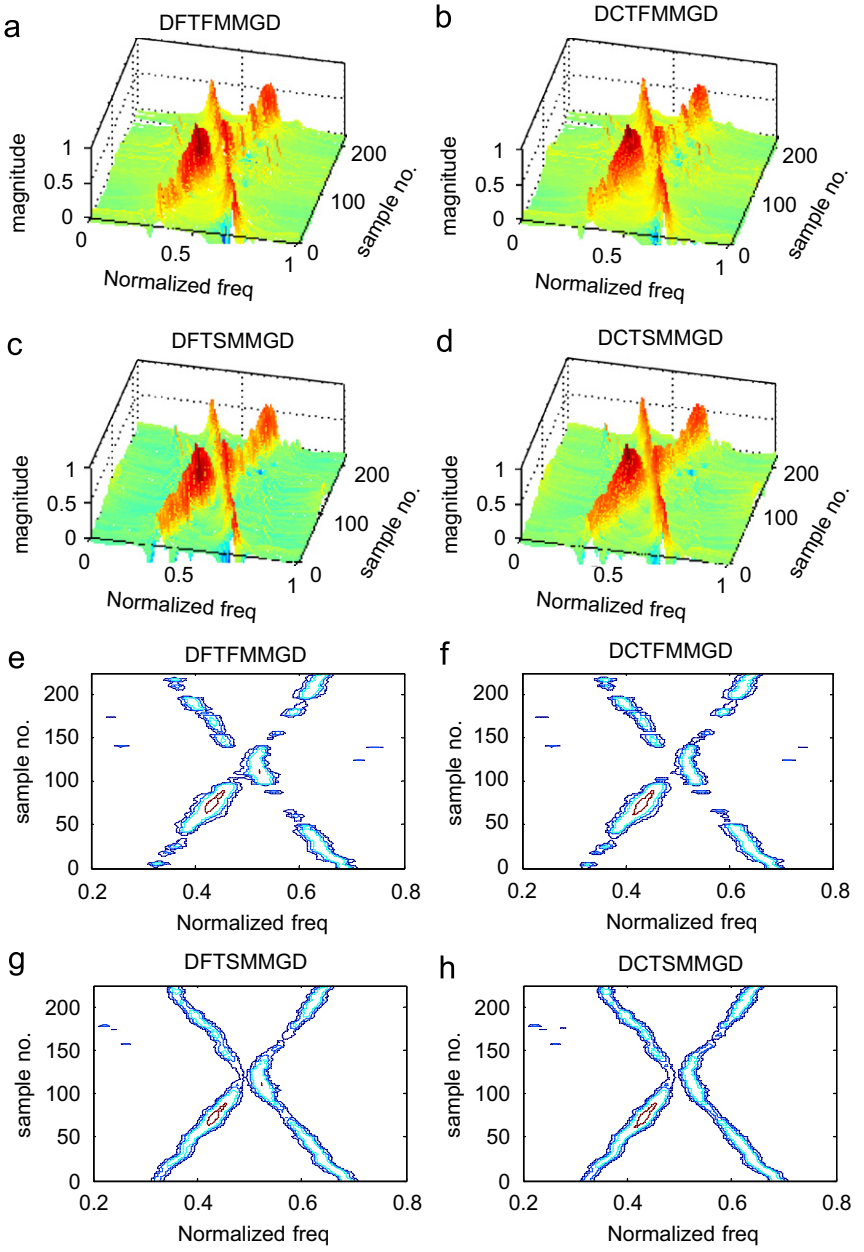

Fig. 3. TFR of a crossing chirp signal with noise by (a)IFFTWVD, (b) IFCTWVD, (c) ISFTWVD, (d) ISCTWVD, and (e)–(h) contours of plots (a)–(d).

where

$$\mathrm{TFR}_{\mathrm{var}}(i,j) = \frac{1}{P}\sum_{k=0}^{P-1}[\mathrm{TFR}_k(i,j) - \mathrm{TFR}_{\mathrm{mean}}(i,j)]^2$$

and $\mathrm{TFR}_{\mathrm{mean}}(i,j) = 1/P\sum_{k=0}^{P-1}\mathrm{TFR}_k(i,j)$, where P is number of segments.

From Table 3 it is observed that, for crossing chirp signal subband MMGD processing has an improvement over fullband MMGD processing of 38.5% and 37% for SD by DFTHWT and DCTHWT, respectively. For sinusoidal chirp signal, subband MMGD processing has an improvement over fullband MMGD processing of 19% and 20% for SD by DFTHWT and DCTHWT, respectively. The SD by DCTHWT has an improvement of 48% over that by DFTHWT for subband MMGD processing for linear chirp signal. This is expected as splitting the band really affects the

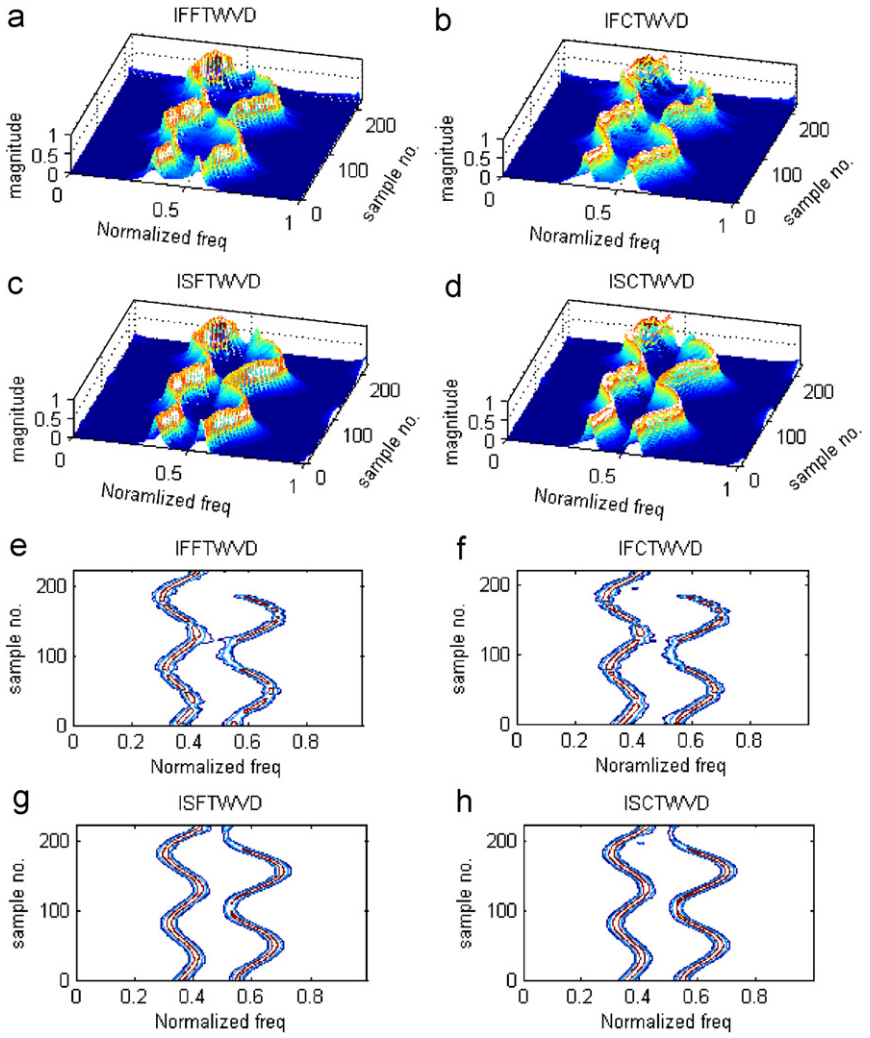

Fig. 4. TFR of sinusoidal chirp signal by (a) IFFTWVD, (b) IFCTWVD, (c) ISFTWVD, (d) ISCTWVD, and (e)–(h) contour plots of (a)–(d).

Table 3
ASSV of different IWVDs for different signals with noise

Signals	SNR (dB)	IFFTWVD	IFCTWVD	ISFTWVD	ISCTWVD
Crossing chirp	4	0.0200	0.0186	0.01230	0.0117
Sinusoidal chirp	8	0.0064	0.0064	0.0052	0.0051

crossing point of the two linear chirps. For sinusoidal chirp practically there is no improvement both for fullband and subband processing, weather the SD is done by using DFTHWT or DCTHWT. This is expected as sinusoidal chirp are well separated, the leakage will be less and also splitting the bands will not have any effect on the performance. These results indicate the reduction in variance achieved by ISCTWVD and hence its performance is superior compared to the other methods considered.

For 2 nonstationary sinusoidal chirp signals $\sin[2\pi\{94+0.64\sin(n/16)\}nT_s]$ and $\sin[2\pi\{160+1.08\sin(n/17)\}nT_s]$ of *different amplitudes* 1 and 0.4,

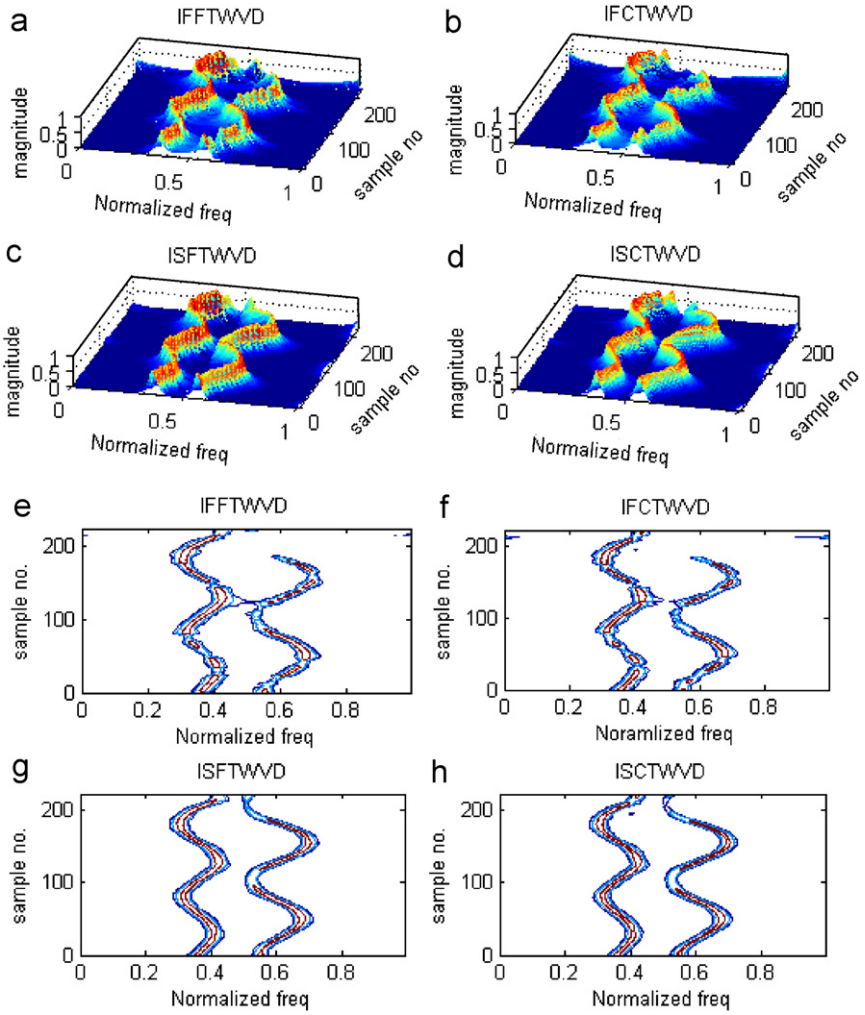

Fig. 5. TFR of sinusoidal chirp signal with white noise by (a) IFFTWVD, (b) IFCTWVD, (c) ISFTWVD, (d) ISCTWVD, and (e)–(h) contour plots of (a)–(d).

respectively, the IWVD obtained by different algorithms are shown in Fig. 6. It is clear that subband MMGD processing is able to detect the low level sinusoidal chirp in the presence of stronger one, *which is not possible by fullband processing*. The ISCTWVD provides better frequency resolution (sharpness of the peaks), detectability, and also continuity of contours compared to the other methods, considered.

For the nonstationary sinusoidal chirp signals of different amplitudes in presence of white noise (SNR = 7 dB) (Fig. 7), the ISCTWVD can detect the weaker signal. Also the floor surface is clean, compared to those of other methods.

In the above example of two sinusoidal chirps also, the SD by splitting signal frequency band into two bands at a frequency, which is midway between the two component frequencies, removes the cross-term. For this example, the individual sinusoidally time varying chirps completely lie in each separate band. In view of this, this example does not have any ill effect of magnitude reduction near the border due to band splitting (as in the case of crossing linear chirps). Hence the SD does not affect the WVD and its contour plots.

As an example for real data analysis, heart rate variability (HRV) data is considered. The frequency content of the heart rate data plays an important role in classifying as normal and abnormal [13]. Wavelet transform, which provides information about both time and frequency, was used for this purpose [14]. This HRV is similar to that of a two

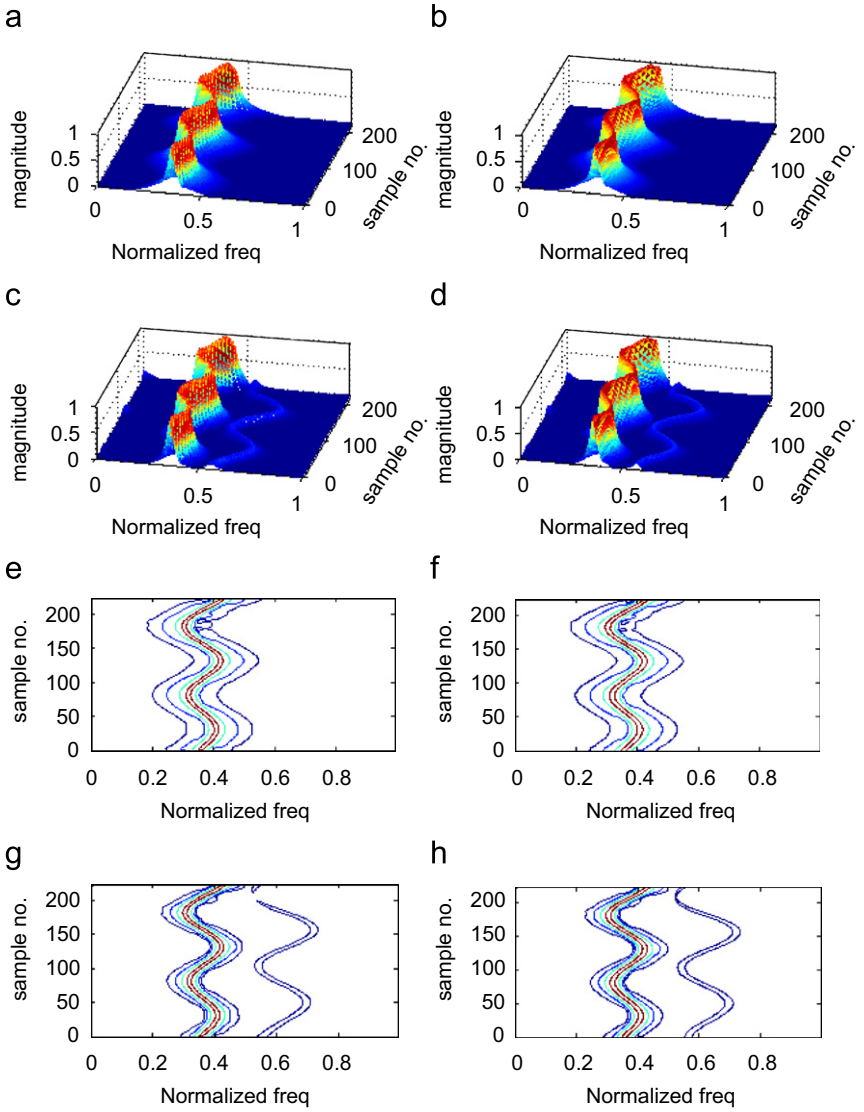

Fig. 6. TFR of sinusoidal chirp signal by (a) IFFTWVD, (b) IFCTWVD, (c) ISFTWVD, (d) ISCTWVD, and (e)–(h) contour plots of (a)–(d).

sinusoidally varying nonstationary chirps considered. The proposed methods are applied to a practical heart rate data. For the normal case, the data has a prominent second component. However for myocardial infraction abnormality, the second component magnitude is very much reduced. Hence mainly for the normal case, the signal is a multicomponent one, with two components and the WVD suffers from crossterm effect.

To retain the computational benefit and simplicity of HWT, the SD should result in a number of bins which is a power of two. To facilitate this, the signals have been preprocessed for sampling rate change. For the normal case, the data is decimated by a factor 2. This expands the spectrum and enables to locate a convenient boundary for splitting the spectrum. The abnormal data is decimated by 3 and interpolated by 2. These modifications do not affect the final result as they have been accounted.

The parameters used are: original data length 512 samples, lag length = 31, number of subbands = 2, cepstral coefficients = 5. For the MMGD processing, the floor level is raised by a factor of 10,000. The cepstral coefficients to be used for subband processing is half that of fullband. The results

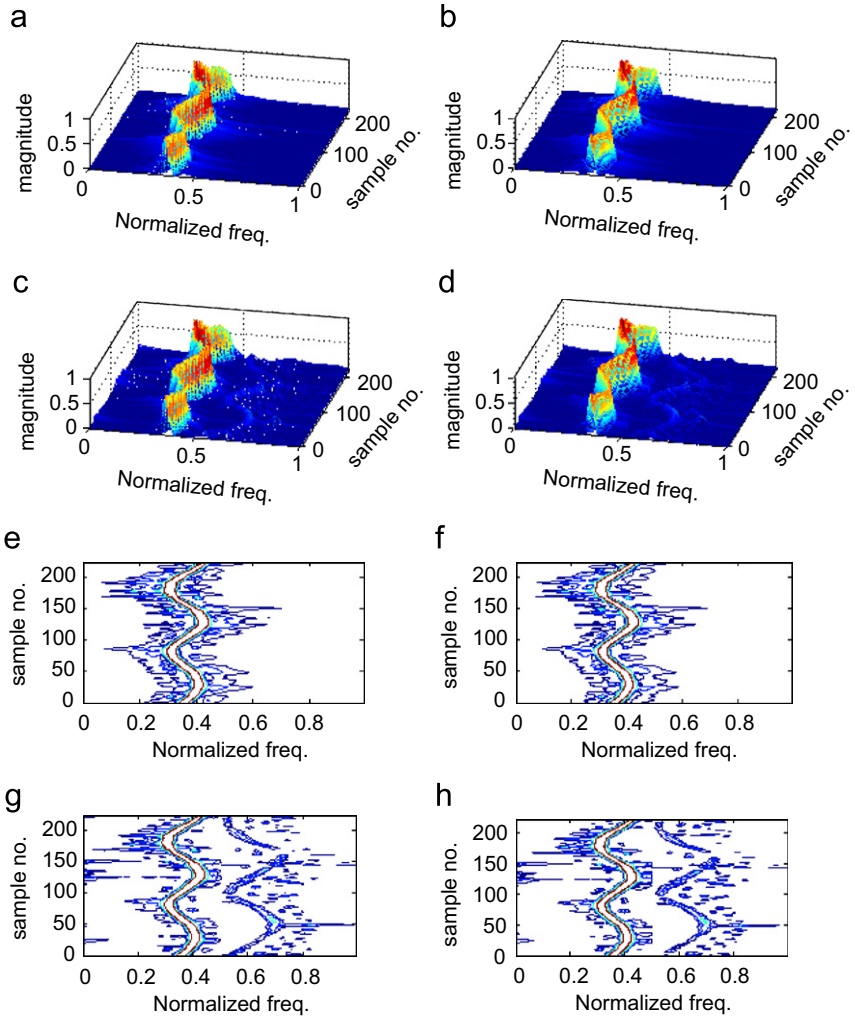

Fig. 7. TFR of sinusoidal chirp signal with white noise by (a) IFFTWVD, (b) IFCTWVD, (c) ISFTWVD, (d) ISCTWVD, and (e)–(h) contour plots of (a)–(d).

presented for subband are with 5 cepstral coefficients as it reduces the unwanted disturbances though the main features of the results are same as with those of 2 coefficients.

Figs. 8(a) and (b) show the WVD (which does not use SD and MMGD) and its contour plots of normal HRV data. The WVD (without any time and frequency smoothing) though provides good time and frequency resolution, it suffers from severe crossterm effect and Gibbs ripple. Hence it is required to remove the crossterm and Gibbs ripple and retain the good features of the WVD. The WVD based on SD and MMGD shown in Figs. 8(a), (c), (e), (g) and (i) and their contour plots Figs. 8(b), (d), (f), (h), and (j) clearly indicate that the crossterm and the Gibbs ripple are almost removed. The WVD plots and their contours based on DFT (Figs. 8(c) and (d)) and DCT (Figs. 8(e) and (f)), which use fullband processing have similar performance. Though the second frequency component has been brought out well with its variations, it is not so with the first component (Figs. 8(b), (d), and (f)). On the other hand, the subband MMGD processing in addition to bringing out the second frequency component variation with an improved frequency resolution (continuity of the contour plot in the in between 150 and 250 samples), it has restored the first frequency component pattern as in the WVD (Figs. 8(b), (h) and (i)). The changes in the frequency of the components may correspond to physiological changes which will be taking place. In the present HRV case, strength of the second

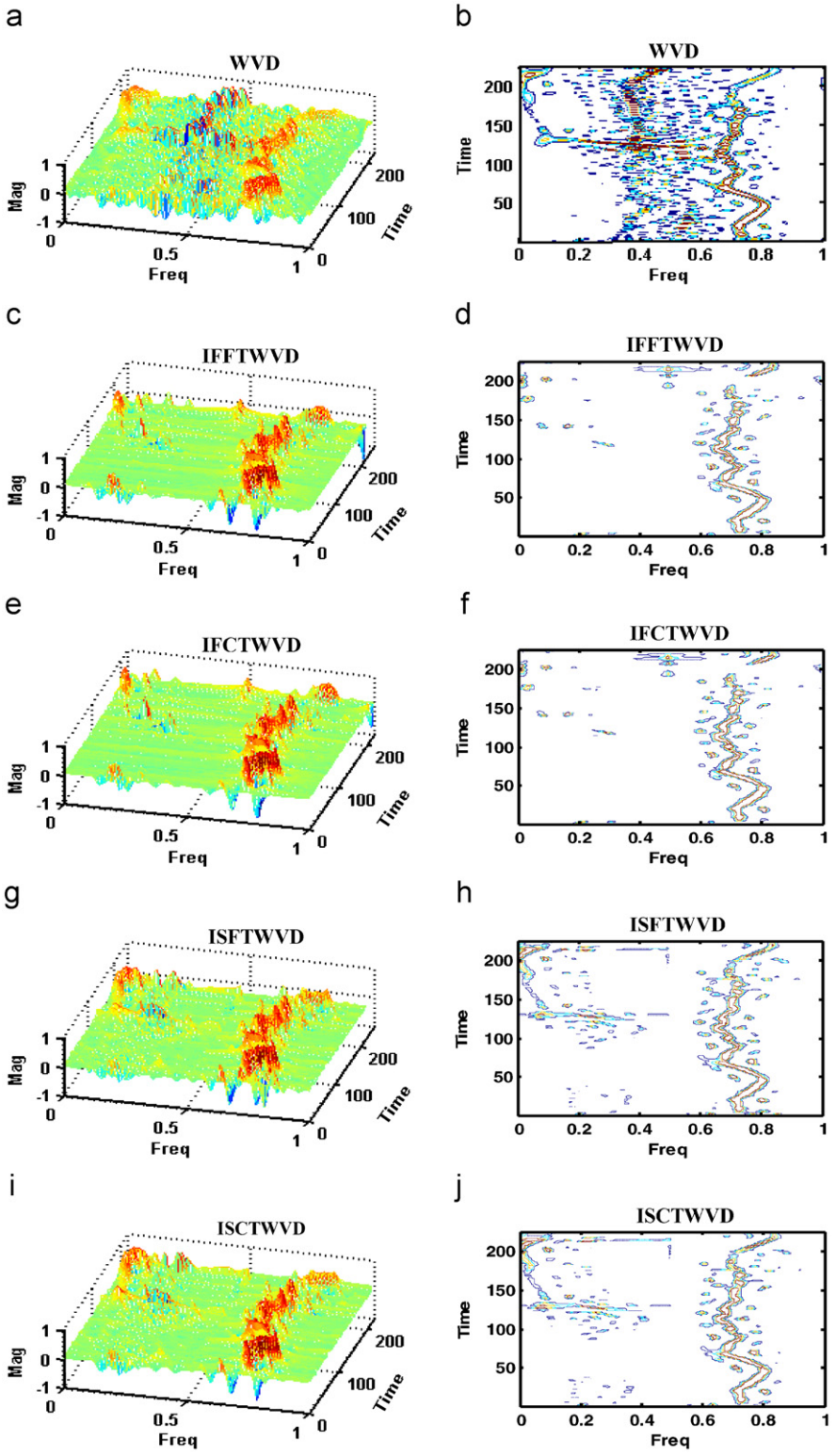

Fig. 8. Normal heart rate data analysis.

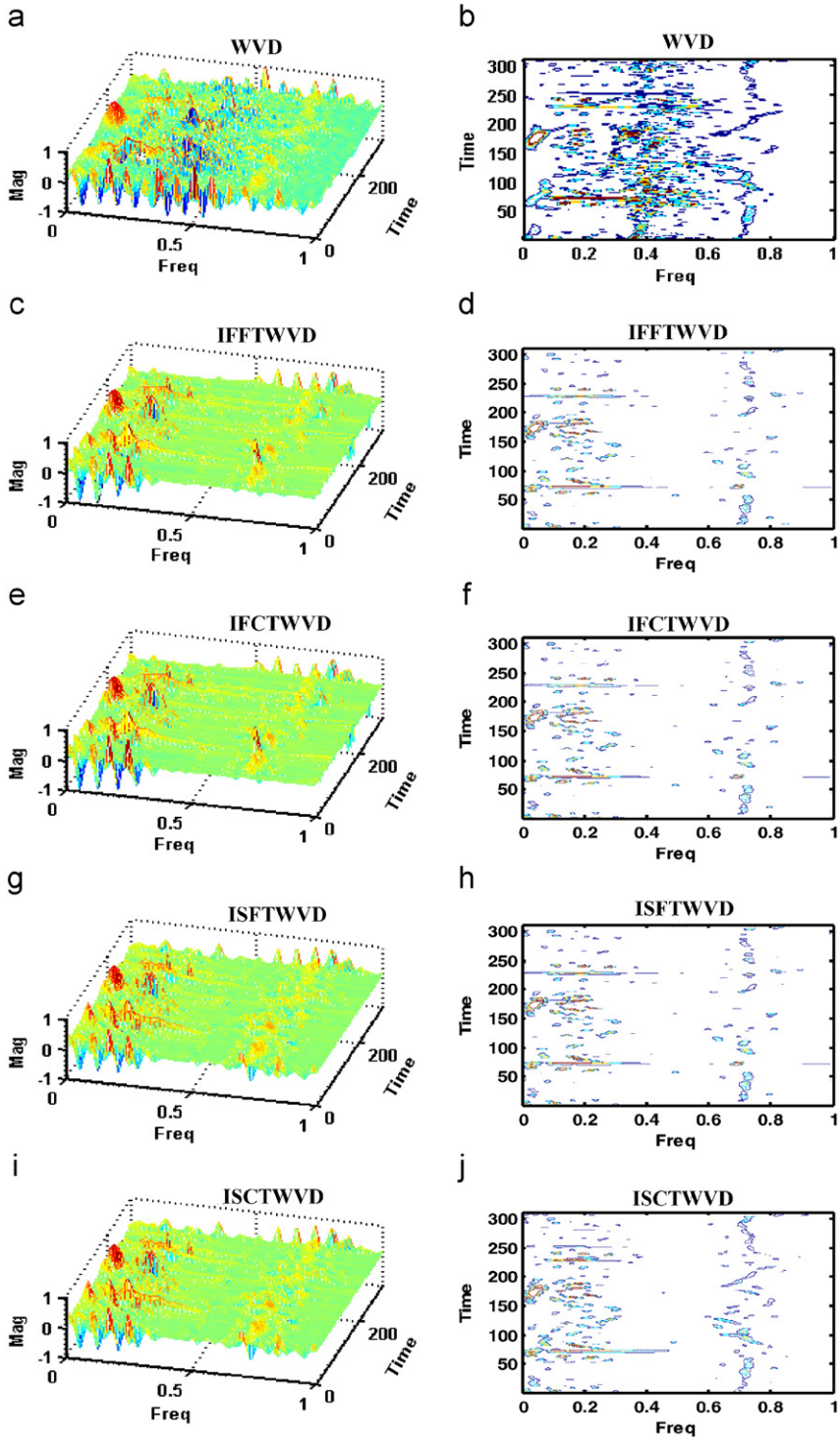

Fig. 9. Abnormal heart rate data analysis.

component relative to that of the first decides about the normal and abnormal classification [13]. From this point of view, the subband processing algorithms seem to have better performance as they have retained the energy level for both the components, throughout the duration considered. However, as

pointed out, the frequency transition from one band to the other may not have brought out well which is not of importance in this case.

The performance of the proposed methods for abnormal HRV data is shown in Fig. 9. Here also, the WVD (without time and frequency smoothing) suffers from severe crossterm and Gibbs ripple effect (Figs. 9(a), (b)). The processing based on SD and MMGD are almost free from crossterm and Gibbs ripple effect (Figs. 9(c)–(i)). The MMGD subband processing has brought out both the components reasonably well compared to those of fullband. Specifically with reference to the second component, the performance of the fullband processing is not good compared to that of subband (Figs. 9(d), (f) and (h), (i)). This is evident from the fullband processing contour plots (Figs. 9(d) and (h)) as they are having too many breaks and lack continuity. The reason for this is that the fullband processing cannot bring out the details of a weak component in the presence of a strong one. From energy point of view, both fullband and subband MMGD processing indicate that the energy of the second component is lower than the first which is the desired result.

In the above cases, it can be observed that the Gibbs ripple is removed while maintaining the frequency resolution of rectangular window by MMGD. The SD by DCT/DFT HWT and subband processing is effective in removing the spurious spectral peaks due to noise while improving the frequency resolution. The MMGD processing in subbands is less affected by neighboring noise components as components are well separated and for the same reason a better frequency resolution is achieved. The SD by HWT removes the crossterms due to noise and the MMGD removes the zeros due to noise in addition to those due to Gibbs ripple. Hence, the MMGD processing in subbands provides an enhanced immunity to noise, compared to that of the others. However, if there are transition paths from one frequency band to another, they are not brought out properly and there can be gaps in the WVD contour plots.

7. Conclusions

A new Wigner–Ville distribution (WVD) with improved performance based on signal decomposition (SD) by DCT/DFT HWT and modified magnitude group delay (MMGD) processing in fullband/subband, is proposed. The HWT decomposes the signal in a simple and computationally efficient way as it involves only grouping of the DCT/DFT coefficients without any explicit decimation operation. The IACR is computed at a *decimated rate* and the overall WVD slice is obtained *by plugging back* the FT of the component IACRs, in their corresponding positions without any explicit interpolation. Thus, it does not require any explicit filtering both for antialiasing and image rejection. DCTHWT is simple as it does not involve complex quantities and in terms of multiplications, the computational load required is less compared to that of DFTHWT. Further, the subband WVDs are computationally efficient than the fullband ones.

The methods are applied to two linearly crossing chirps, two sinusoidally varying chirps about two frequencies and to real HRV data. The SD by HWT removes the very existence of crossterms and the MMGD removes the autocorrelation truncation effects, without using any window function. The proposed WVDs compared to the Cohen's class PWVD, have both improved frequency and time resolution and obey the desired TFR properties better due to the absence of time and frequency smoothing. As MMGD is more effective in subband processing, it provides increased frequency resolution and signal to noise ratio. The performance of the proposed algorithm based on DCT is better in terms of variance and frequency resolution than that of DFT. Compared to fullband WVD, the subband WVDs are computationally efficient and have significantly better detectability (of low-level signal in the presence of high-level one) and variance. The SD though provides a proper information about frequency changes with in the bands, it fails to do so for frequency transitions across the bands if any.

Acknowledgements

The authors thank Mrs. Padma Mudhuranath, for having done the English language correction of the manuscript. They thank Mr. P.V.S. Naidu for providing the HRV data and its details. In processing the HRV data, the efforts of Mr. P. Sandeep, M. Tech. Project student of NITK, are highly appreciated.

References

[1] J. Jeong, W.J. Williams, Kernel design for reduced interference distributions, IEEE Trans. Signal Processing 40 (2) (1992) 402–412.

[2] F. Sattar, G. Salomonsson, The use of a filter bank and the Wigner–Ville distribution for time–frequency representation, IEEE Trans. Signal Processing 47 (6) (June 1999) 1776–1783.

[3] (a) S.V. Narasimhan, E.I. Plotkin, M.N.S. Swamy, Power spectrum estimation of complex signals and its application to Wigner–Ville distribution: a group delay approach, Sadhana 23 (Part 1) (1998) 57–71;
(b) S.V. Narasimhan, M.B. Nayak, Improved Wigner–Ville distribution performance by signal decomposition and modified group delay, Signal Processing 83 (2003) 2523–2538.

[4] B. Yegnanarayana, H.A. Murthy, Significance of group delay functions in spectral estimation, IEEE Trans. Signal Processing 40 (9) (September 1992) 2281–2289.

[5] D.E. Newland, Wavelet analysis of vibration, Part-1: theory, J. Vib. Acoust. Trans. ASME 116 (1994) 409–416.

[6] G.R. Reddy, V.V. Rao, Group delay functions for complex signals, Signal Processing 12 (1987) 5–15.

[7] S.V. Narasimhan, E.I. Plotkin, M.N.S. Swamy, Power spectrum estimation of complex signals: group delay approach, Electron. Lett. 35 (5) (December 1999) 2182–2184.

[8] S.V. Narasimhan, B.K. Shreyamsha Kumar, Harmonic wavelet transform signal decomposition and modified group delay for improved Wigner–Ville distribution, in: International Conference on Signal Processing and Communication (SPCOM-2004), Bangalore, India.

[9] S.V. Narasimhan, M. Harish, Spectral estimation based on subband decomposition by harmonic wavelet transform and modified group delay, in: IEEE International Conference on Signal Processing and Communication (SPCOM-04), December 2004, Indian Institute of Science, Bangalore, India.

[10] (a) J.S. Lim, Two-Dimensional Signal and Image Processing, Prentice-Hall, Englewood Cliffs, NJ, 1990 (Chapter 3);
(b) S.V. Narasimhan, M. Harish, Spectral estimation based on discrete cosine transform and modified group delay, Signal Processing 86 (7) (July 2006) 1586–1596.

[11] (a) S.V. Narasimhan, M. Harish, Discrete cosine harmonic wavelet transform and its application to subband spectral estimation using modified group delay, in: Proceedings of the Conference in Honor of Dr. B.R. Pai, National Aerospace Laboratories, Bangalore, India, November 2004;
(b) S.V. Narasimhan, M. Harish, A.R. Haripriya, Discrete cosine harmonic wavelet transform: application to signal compression and subband spectral estimation using modified group delay, Signal, Image & Video Processing (submitted for publication).

[12] K.R. Rao, P. Yip, Discrete cosine transform, algorithms, advantages, applications, United Kingdom Edition published by Academic Press Limited, London.

[13] G.A. Mayers, et al., Power spectral analysis of heart rate variability data in sudden cardiac death: comparison to other methods, IEEE Biomed. Eng. 33 (12) (1986) 1149–1155.

[14] C. Medigue, et al., Discrete wavelet transform applied heart rate variability analysis in iron deficient anemic infants, in: Proceedings of the 19th International Conference on IEEE/EMBS, October 30–November 2, 1997, Chicago, IL, USA, pp. 1613–1616.